Clays from the Bay of Naples (Italy): New insight on ancient and traditional ceramics

Alberto De Bonis [a],*, Giuseppe Cultrone [b], Celestino Grifa [c], Alessio Langella [c], Vincenzo Morra [a]

[a] *Dipartimento di Scienze della Terra, dell'Ambiente e delle Risorse (DiSTAR), Università Federico II, Via Mezzocannone 8, 80134 Napoli, Italy*
[b] *Departamento de Mineralogía y Petrología, Universidad de Granada, Avda. Fuentenueva s/n, 18002 Granada, Spain*
[c] *Dipartimento di Scienze e Tecnologie, Università del Sannio, Via dei Mulini 59/A, 82100 Benevento, Italy*

Abstract

The features of two clayey raw materials from the Bay of Naples and their fired products were investigated via minero-petrographic and physical techniques.

Clay preparation and firing dynamics were performed following a process similar to that performed by ancient and traditional potters. A high-CaO marine clay from Ischia was mixed with different amounts of volcanic temper in order to replicate most common ware. These mixtures show a fair mechanical resistance starting from relatively low firing temperatures (>850 °C). The addition of temper resulted in different technological characteristics. A low-CaO weathered pyroclastics from the Sorrento Peninsula was prepared to simulate heat resistant and refractory ceramics. Fired products are characterised by a less resistant ceramic body up to 1000 °C compared to Ischia ceramics. Despite worse strength these ceramics show a porous structure, yielding better refractory performances.

1. Introduction

The objective of this study is to understand the technological potential of two different types of clayey raw materials for manufacturing ceramics, with particular attention to archaeological pottery and traditional technologies. Experimental firing was performed with two raw materials from the Bay of Naples area, which were selected from among a set of already characterised samples from the Campania region.[1] Our attention was focused on the Bay of Naples because the area is renowned for its rich archaeological record and for the presence of attested pottery production centres (e.g., Ischia, Cuma, Pompeii, Neapolis).[1–7] The two clays come from two different sites on the bay, the island of Ischia and the Sorrento Peninsula respectively,

and they are characterised by their different geological origin and minero-petrological composition. In particular, we considered the calcium oxide (CaO) concentration as a key feature, since it provides peculiar technological properties to the end-products.[8–11]

The raw material collected in the island of Ischia is a high-CaO clay (hereafter *HCC*; CaO > 6 wt.% after Maniatis and Tite[9]) and, despite the volcanic nature of the island, it is a marine sediment now outcropping at approximately 600 m above sea level following the Mt. Epomeo resurgence.[12] The historical and archaeological importance of Ischia is well known. The island is considered to be one of the first and most important production sites for pottery in the Bay of Naples, especially in the Hellenistic period, and its clay was most likely exported to supply the workshop on the coast in the Graeco-Roman period.[2,3,7,13] Pottery production on the island of Ischia and exportation of raw material as well are documented from the 16th to the 19th century A.D.[14]

The raw material from the Sorrento Peninsula is a low-CaO clay (hereafter *LCC*; CaO < 6 wt.%) deriving from weathered

* Corresponding author. Tel.: +39 081 2538115.
  E-mail addresses: alberto.debonis@unina.it, axdybz@gmail.com
(A. De Bonis), cultrone@ugr.es (G. Cultrone), celgrifa@unisannio.it (C. Grifa),
langella@unisannio.it (A. Langella), vimorra@unina.it (V. Morra).

pyroclastic deposits. This raw material is currently exploited by a traditional ceramic workshop in Maiano, a small village of Sant'Agnello (Naples), to produce bricks, mainly used to build wood-burning ovens and renowned for their refractory properties.[1]

In order to optimise the experimental procedures, the mix design and the ceramic test pieces were fired at different temperatures under oxidising conditions. Clay bodies were prepared according to the results from previous studies on Campanian wares (e.g., use of volcanic temper and its amount for specific ceramic classes),[5,6] as well as the knowledge of today's traditional craftsmen.

The Ischia clay was used either in the condition in which it was found or mixed with different percentages in weight of volcanic temper from the Campi Flegrei.

The clay body containing 0% or 10% of temper replicated the characteristics of fine ware,[4,7,11,15,16] 20% of temper was added to roughly simulate most common ware, amphorae, or bricks,[4,15] while 30% of temper was used to obtain coarse ware and bricks.[5,6,15,17,18]

The Sorrento clay was used to replicate heat resistant ceramics products (e.g., cookware) and refractory bricks, as this raw material has features suitable for this kind of product, namely low-CaO composition and high coarse grain content.[19]

The ceramic test pieces were analysed via mineropetrophysical methods to obtain useful data for the interpretation of ancient ceramics in terms of technology and provenance, as well as to improve the existing knowledge on traditional ceramic manufacturing.

2. Experimental procedure

Ceramic test pieces were prepared using two clayey materials from the island of Ischia (IS; UTM coordinates: 33 T 408,283 mE 4,509,355 mN) and from the Sorrento Peninsula (SO; UTM coordinates: 33 T 449,430 mE 4,497,255 mN). Major details concerning their geological context are provided elsewhere.[1]

The volcanic beach sand used as temper (AQM; UTM coordinates: 33 T 419,359 mE 4,516,746 mN) in IS mixtures was sampled from the beach of *Acquamorta* in Monte di Procida (Campi Flegrei).

The grain size of clayey raw materials was determined by a wet method using standard sieves,[20] for the determination of the $>74 \mu m$ fraction (No. 200 ASTM sieve). The passing fraction was complementarily analysed by means of a sedimentation technique,[21] allowing the evaluation of the $<2 \mu m$ (clay fraction). The grain size of the temper was evaluated via a dry sieving method.[22] The Atterberg limits[23–25]: liquid limit (w_L), plastic limit (w_P), shrinkage limit (w_S), and plasticity index $(PI = w_P - w_L)$, were also estimated to define the critical values of water controlling the different rheological stages of clayey sediments. The organic matter content was determined on predried samples (overnight at $110\,^\circ C$) through a loss on ignition technique, consisting of heating at $450\,^\circ C$ over 72 h in a muffle furnace.[26]

Four types of clay bodies were prepared with the clays from Ischia. The first type was prepared without any temper addition (IS), while the other three types were clay/temper mixtures prepared with 10% (IS-A), 20% (IS-B), and 30% (IS-C) in weight of temper. Weathered pyroclastics from Sorrento (SO) were prepared without any temper addition, owing to the natural abundance of coarse inclusions.

The clay bodies were prepared with extreme accuracy, leaving the clays in water for several hours until a semi-liquid consistency was obtained. Successively, the samples were dried until the proper plasticity was achieved. After that, the right amount of temper (10%, 20%, or 30% of clay dry weight) was added and the clay bodies were accurately kneaded to eliminate air excess. Samples were fashioned in a wooden mould ($32\,cm \times 24\,cm \times 4\,cm$) and cut with a metal wire to obtain eight raw bricks ($12\,cm \times 8\,cm \times 4\,cm$) per type of paste. Accurate drying of raw bricks was achieved in laboratory after 10 days under controlled thermo-hygrometric conditions ($T = 25\,^\circ C$, $HR = 50\%$).

Firing was performed under an oxidising atmosphere in an electric muffle furnace (Nabertherm HTCT 08/16) equipped with an electronic controller (Nabertherm P330). Control of the correct calibration of the firing temperature of the kiln was performed via the pyrometric cones (Orton type) method.[27] The firing process was reproduced to be similar to that which is currently performed by traditional potters from the Sant'Agnello workshop, who use a wood-firing cycle of approximately 7–8 h. A slow initial heating rate ($1.5\,^\circ C\,min^{-1}$), followed by a higher heating rate ($3\,^\circ C\,min^{-1}$) starting at $200\,^\circ C$ to the maximum T, was followed by a soaking time of 90 min and then by a cooling according to the free drift of the switched off kiln. The bricks were quickly immersed in water after firing to set free from $Ca(OH)_2$ or CaO excess if present.[28]

Mineralogical analyses of the raw materials (clays and temper) and fired ceramics were carried out by means of X-ray powder diffraction (XRPD). A McCrone Micronising Mill was used to obtain a very fine powder ($\sim 10 \mu m$).[29] The data were acquired with a PANalytical X'Pert PRO 3040/60 PW diffractometer (CuKα radiation, 40 kV, 40 mA, scanning interval 4–80° 2θ, equivalent step size 0.017° 2θ, equivalent counting time 120 s per step, RTMS X'Celerator detector). Identification of the clay phases was performed on oriented aggregates on fraction below $2 \mu m$. The data were obtained with a Philips PW 1710 diffractometer (CuKα radiation, 30 kV, 40 mA, scanning interval 3–35° 2θ, step size 0.020° 2θ, counting time 2 s per step) on air-dried samples and after thermo-chemical treatments (ethylene glycol solvation, $550\,^\circ C$ heating). A relative percentage of mixed layer phyllosilicates and the statistical layer ordering variable (Reichweite; R) was also estimated according to Moore and Reynolds,[30] meaning that the mixed layer minerals may be randomly distributed ($R = 0$) or ordered ($R \geq 1$).

X-ray fluorescence spectrometry (XRF, PANalytical Axios instrument) allowed us to obtain chemical analyses of major oxides (wt.% of SiO_2, TiO_2, Al_2O_3, Fe_2O_3, MnO, MgO, CaO, Na_2O, K_2O, P_2O_5) and trace elements (ppm of Rb, Sr, Y, Zr, Nb, Ba, Cr, Ni, Sc, V) of the raw materials and ceramics (detection

limits according to Melluso et al.[31]). Loss on ignition (LOI) was determined by pre-drying 1 g of powder of the sample overnight at 110 °C and then heating the sample to 1000 °C.

Polarised light microscopy (PLM) was performed with a Leitz Laborlux 12 POL microscope to describe the petrographic composition of the ceramics. Modal analyses (based on ca. 4000 points per section) were carried out with Leica Q Win software (3.5.1 version) on PLM images acquired with a Leica DFC280 camera.

Scanning electron microscopy (SEM) observations of ceramic microstructures were performed on fresh fractured samples with a JEOL 5310 instrument; micro-chemical analyses were carried out with the same instrument fitted with an energy dispersive X-ray spectrometer (EDS; Oxford INCA X-act; 15 kV, 50–100 mA, spot-size 15–17 μm, acquisition time 50 s) on backscattered electrons (BSE) images of carbon-coated thin sections. The data were elaborated by an INCA X-stream pulse processor, and the calibration was made with the following standards: strontianite (Sr), baryte (Ba), rutile (Ti), vanadium (V), Cr_2O_3 (Cr), rhodonite (Mn), nickel (Ni). Images of most of the representative samples were acquired by high resolution field emission scanning electron microscopy (FESEM; Leo Gemini 1530).

Pore access size and its evolution with firing, as well as pore volume, were determined by mercury intrusion porosimetry (MIP). Freshly cut samples of ∼2 cm³ which had been pre-dried for 24 h at 110 °C were analysed with a Micrometrics AutoPore III 9410 porosimeter.

Parameters associated to both fluid uptake and transport through the pore system were determined by hydric tests. Free[32] and forced[33] water absorption and drying[34] were measured by weighing the samples at regular intervals. The average weight of three cubic pieces (3 cm side) per sample was considered to obtain statistical significance of the data. Free (A_l) and forced (A_f) water adsorption, pore connectivity (A_x), open porosity (O_p), absorption (C_a) and saturation (C_s) coefficients, apparent (ρ_a) and (ρ_r) real densities, and drying index (D_i) were also calculated.[10]

Ultrasound testing was performed with a 100 MHz pulser/receiver (Panametrics NDT 5058PR) coupled with an oscilloscope (Tektronix TDS 3012B) to measure the velocity of propagation (V_p, V_s) of elastic waves along the three orthogonal directions of cubic test pieces (3 cm/side). Average measures of three test pieces of each sample were considered. The test[35] was performed under controlled thermo-hygrometric conditions ($T = 20$ °C, $HR = 50\%$). These data were used to obtain information on the degree of compactness of the ceramic materials.[36] The velocities of P and S waves were used to determine elastic moduli for non-destructive characterisation of heterogeneous materials,[37] and the Young's modulus (E), bulk modulus (K), and shear modulus (G) were calculated.

Infrared thermography (IRT) was performed to measure heat propagation in representative samples, which were fired at the lowest, intermediate, and maximum T (700, 900, 1100 °C). Tests were made under controlled thermo-hygrometric conditions ($T = 25$ °C, $HR = 50\%$), by heating prismatic test pieces (6.0 cm × 3.5 cm × 1.5 cm) on a hot plate (50 °C) at a distance of
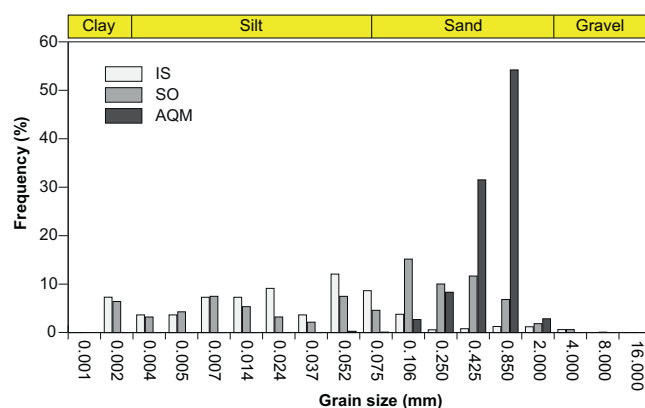

Fig. 1. Grain size distribution of IS and SO clayey raw materials and AQM temper.

30 cm from the lens of the thermographic camera (FLIR SC660). Each test consisted of a heating phase of 20 min followed by a 40 min cooling phase. Qualitative evaluation of heat propagation was carried out by measuring the displacement of a 40 °C isotherm at regular intervals (5 min) all along the surfaces of the test pieces by means of a video analysis software (Kinovea, version 0.8.7).

3. Results and discussion

3.1. Physical, chemical and mineralogical characteristics of raw materials

Data concerning the two clayey raw materials used for the experimental firing (IS and SO samples) were taken from our previous work on the petrophysical characterisation of Campanian clays,[1] where IS and SO samples were reported as IS6 and SO1, respectively.

The particle size of the clayey sample from Ischia (IS) was mainly comprised of the silt range (44%), with 23% being represented by sand and 31% by clay; the gravel fraction was negligible. The SO sample showed a grain size distribution quite similar to the IS sample, although it was richer in coarse fraction (Fig. 1). In the weathered pyroclastic sample from Sorrento (SO) sand was the prevailing fraction (53%), silt was approximately 33%, and clay only constituted 11%; gravel was roughly 2.5% (Table 1). The volcanic beach sand used as temper (AQM) in the IS mixtures was almost completely formed by sand (97%). It showed a clear unimodal distribution with the main peak in the coarse sand at 0.850 mm (Fig. 1).

The Atterberg limits (Table 1) calculated on the two raw clays (IS and SO) showed a similar liquid limit ($w_L \sim 54.0\%$). The plastic limit (w_P) varied from 29.5% (IS) to 39.5% (SO). A higher plasticity index (PI) was evaluated for IS (24.5%) with respect to SO (14.4%). The shrinkage limit (w_S) was much higher for SO (31.9%) than IS (14.6%).

From a chemical point of view (Table 2) the IS sample was an *HCC* (CaO content 9.70 wt.%), while the SO sample was an *LCC* (CaO content 2.57 wt.%). The addition of temper (AQM) only caused slight variations in the compositions of the clay

Table 1
Grain size of raw materials (clays and temper) and Atterberg limits of raw clays: w_L, liquid limit; w_P, plastic limit; w_S, Atterberg shrinkage limit; PI: plasticity index. Organic matter content is also reported.

	IS	SO	AQM
Gravel (%)	1.8	2.5	3.0
Sand (%)	23.2	53.5	97.0
Silt (%)	44.0	33.0	–
Clay (%)	31.0	11.0	–
w_L (%)	53.99	53.97	–
w_P (%)	29.48	39.53	–
w_S (%)	14.62	31.94	–
IP (%)	24.51	14.44	–
Organic matter (%)	5.95	7.59	–

bodies, likely determined by an alkali (K_2O, Na_2O) enrichment due to the composition (mostly trachytic) of Phlegraean products[38] (Table 2). The two clayey raw materials showed an organic matter content of 5.95 wt.% (IS) and 7.59 wt.% (SO), which accounted for the brownish colour of the two samples.

XRPD analyses (Table 3) showed that the IS raw material was composed of very abundant quartz, frequent feldspars, abundant calcite, and minor dolomite; scarce pyroxene was also recorded (Fig. 2a). Clay minerals were represented by illite/mica (muscovite, biotite), kaolinite, chlorite, and illite-smectite mixed-layer with an illite percentage of approximately 50% and layer ordering ($R = 0$). The weathered pyroclastics (SO) showed abundant feldspars and, frequent quartz, and pyroxene. The presence of amorphous/glass phase was also inferred from the presence of a background noise represented by illite/muscovite and a lesser amount of dehydrated halloysite, a common phase of several Campanian weathered pyroclastics.[39] AQM was mainly composed of feldspars and minor amounts

of pyroxene, mica, and analcime, the latter deriving from the weathering of volcanic glass.[40]

The addition of AQM modified only to a lesser extent the bulk mineralogical composition of the IS clays. A slight decrease in calcite, dolomite, and quartz content, along with a slight increase in feldspars and pyroxene, was noticed with high percentage of temper (20%, 30%; Table 3).

3.2. Fired ceramics

3.2.1. Chemical and mineralogical composition

Slight differences in chemical composition between raw and fired samples were observed, thus suggesting an almost iso-chemical firing process. As expected, only LOI values showed a significant decrease (Table 2).

From a mineralogical point of view the IS ceramics were all richer in quartz than SO samples, thus supporting the higher SiO_2 content observed via XRF. Firing caused the decomposition of phyllosilicates and carbonates whenever present (Table 3). Chlorite was still barely noticeable in IS ceramics at 700 °C showing a slight shift towards lower d-values (Fig. 2a). The dehydroxylated illite-like phase in both ceramic samples progressively reduced in concentrations as the firing temperature increased, until it disappeared only over 1000 °C (Fig. 2a and b). In the SO ceramics, higher amounts of ∼10 Å illite/mica phase were detected, which strongly decreased at maximum T.

When carbonates were present (IS ceramics), calcite decreased starting from 800 °C and was still detected in traces at 1000 °C; at 700 °C the dolomite concentration was already in traces because its decomposition to CaO and MgO starts at temperatures lower than those of calcite breakdown.[41] The persistence of the illite-like phases and calcite at temperatures higher than those expected (∼900 °C for illite and ∼850 °C

Table 2
Chemical analysis (XRF) of major oxides (wt.%, recalculated to 100% on a LOI-free basis), trace elements (ppm) and LOI (loss on ignition, wt.%) of raw clays, of the 950 °C fired ceramics, and of the temper. Abbreviation: <LLD, less than the lower limit of detection of the instrument.

	IS dry	IS 950	IS-A dry	IS-A 950	IS-B dry	IS-B 950	IS-C dry	IS-C 950	SO dry	SO 950	AQM
SiO_2	60.00	59.73	59.61	59.24	59.91	59.69	60.36	59.97	57.98	58.04	61.23
TiO_2	0.77	0.75	0.78	0.75	0.77	0.74	0.74	0.74	0.90	0.94	0.66
Al_2O_3	15.83	15.41	15.93	15.73	15.99	15.68	15.99	15.73	24.15	22.10	16.29
Fe_2O_3	6.13	5.90	5.99	6.00	5.90	5.86	5.72	5.81	7.38	7.70	4.98
MnO	0.14	0.14	0.14	0.14	0.13	0.13	0.13	0.13	0.19	0.19	0.12
MgO	2.94	3.29	2.91	3.17	2.86	2.99	2.76	2.85	1.86	2.41	1.93
CaO	9.70	9.77	9.67	9.61	9.07	8.93	8.40	8.37	2.57	3.32	4.29
Na_2O	0.86	1.36	1.02	1.47	1.16	1.67	1.33	1.88	0.79	1.13	3.25
K_2O	3.47	3.50	3.79	3.75	4.06	4.16	4.41	4.36	4.04	4.02	7.08
P_2O_5	0.15	0.15	0.15	0.14	0.15	0.15	0.16	0.15	0.14	0.14	0.18
Total	100.00	100.00	100.00	100.00	100.00	100.00	100.00	100.00	100.00	100.00	100.00
LOI	12.07	1.55	10.43	1.25	9.42	0.86	8.44	0.86	10.90	0.65	1.73
Rb	160	160	164	169	168	164	169	186	175	152	193
Sr	234	235	275	273	301	290	327	365	396	377	507
Y	27	29	28	28	25	27	25	29	40	35	19
Zr	263	271	265	272	261	259	257	282	359	369	245
Nb	27	29	30	31	30	29	31	34	54	54	35
Ba	369	364	419	412	435	441	470	520	1010	1080	712
Cr	74	70	63	70	65	58	49	54	34	69	<LLD
Ni	41	39	38	37	35	34	21	29	26	23	5
Sc	18	14	21	18	17	14	22	12	10	12	6

Table 3

Mineralogical composition (XRPD) of raw materials (clay and temper) and fired ceramics. XXXX, very abundant; XXX, abundant; XX, frequent; X, scarce. Abbreviations: Ill-Sm, illite-smectite mixed layer; Kao, kaolinite; Chl, chlorite; dHall, dehydrated halloysite; Anl, analcime. Colour of samples from Munsell Soil Colour Chart was also reported.

	Quartz	Calcite	Dolomite	Feldspar	Hematite	Melilite	Pyroxene	Illite/mica	Mullite	Other	Colour
IS dry	XXXX	XXX	X	XX	–	–	X	XXX	–	Ill-Sm, Kao, Chl	2.5YR 6/3 (light yellowish brown)
IS 700	XXXX	XXX	Traces	XX	Traces	–	X	XX	–	–	7.5YR 6/6 (reddish yellow)
IS 800	XXXX	XX	–	XX	Traces	–	X	XX	–	–	7.5YR 6/6 (reddish yellow)
IS 850	XXXX	X	–	XX	Traces	Traces	X	X	–	–	7.5YR 6/6 (reddish yellow)
IS 900	XXXX	X	–	XX	Traces	Traces	X	X	–	–	5YR 6/6 (reddish yellow)
IS 950	XXXX	X	–	XX	X	X	X	Traces	–	–	5YR 6/6 (reddish yellow)
IS 1000	XXXX	Traces	–	XX	X	X	X	Traces	–	–	5YR 5/6 (yellowish red)
IS 1100	XXXX	–	–	XXX	X	Traces	XX	–	–	–	5YR 5/4 (reddish brown)
IS-A dry	XXXX	XXX	X	XX	–	–	X	XXX	–	–	2.5YR 6/3 (light yellowis brown)
IS-A 700	XXXX	XXX	Traces	XX	Traces	–	X	XX	–	–	7.5YR 6/6 (reddish yellow)
IS-A 800	XXXX	XX	–	XX	Traces	–	X	XX	–	–	5YR 5/5 (yellowish red)
IS-A 850	XXXX	X	–	XX	Traces	Traces	X	X	–	–	7.5YR 6/6 (reddish yellow)
IS-A 900	XXXX	X	–	XX	Traces	Traces	X	X	–	–	5YR 6/6 (reddish yellow)
IS -A 950	XXXX	X	–	XX	X	X	X	Traces	–	–	5YR 6/6 (reddish yellow)
IS-A 1000	XXXX	Traces	–	XX	X	X	X	Traces	–	–	5YR 5/6 (yellowish red)
IS-A 1100	XXXX	–	–	XXX	X	Traces	XX	–	–	–	5YR 5/4 (reddish brown)
IS-B dry	XXX	XX	Traces	XXX	–	–	XX	XXX	–	–	2.5YR 5/3 (light olive brown)
IS-B 700	XXX	XX	–	XXX	Traces	–	XX	XXX	–	–	10YR 6/6 (brownish yellow)
IS-B 800	XXX	XX	–	XXX	Traces	–	XX	XX	–	–	7.5YR 6/6 (reddish yellow)
IS-B 850	XXX	X	–	XXX	Traces	Traces	XX	XX	–	–	5YR 6/6 (reddish yellow)
IS-B 900	XXX	X	–	XXX	Traces	Traces	XX	X	–	–	5YR 6/6 (reddish yellow)
IS-B 950	XXX	Traces	–	XXX	X	X	XX	Traces	–	–	5YR 6/6 (reddish yellow)
IS-B 1000	XXX	–	–	XXX	X	X	XX	Traces	–	–	5YR 5/6 (yellowish red)
IS-B 1100	XXX	–	–	XXXX	X	Traces	XXX	–	–	–	7.5YR 5/4 (brown)
IS-C dry	XXX	XX	Traces	XXX	–	–	XX	XXX	–	–	2.5YR 5/3 (light olive brown)
IS-C 700	XXX	XX	–	XXX	Traces	–	XX	XXX	–	–	10YR 6/4 (light yellowish brown)
IS-C 800	XXX	XX	–	XXX	Traces	–	XX	XX	–	–	7.5YR 6/6 (reddish yellow)
IS-C 850	XXX	X	–	XXX	Traces	Traces	XX	XX	–	–	5YR 6/6 (reddish yellow)
IS-C 900	XXX	X	–	XXX	Traces	Traces	XX	X	–	–	5YR 6/6 (reddish yellow)
IS-C 950	XXX	Traces	–	XXX	X	X	XX	Traces	–	–	5YR 6/6 (reddish yellow)
IS-C 1000	XXX	–	–	XXX	X	X	XX	Traces	–	–	5YR 5/6 (yellowish red)
IS-C 1100	XXX	–	–	XXXX	X	Traces	XXX	–	–	–	7.5YR 5/4 (brown)
SO dry	XX	–	–	XXX	–	–	XX	XXXX	–	dHall	10YR 4/2 (dark greyish brown)
SO 700	XX	–	–	XXX	Traces	–	XX	XXXX	–	–	7.5YR 7/4 (pink)
SO 800	XX	–	–	XXX	Traces	–	XX	XXX	–	–	7.5YR 6/6 (reddish yellow)
SO 850	XX	–	–	XXX	Traces	–	XX	XXX	–	–	7.5YR 6/6 (reddish yellow)
SO 900	XX	–	–	XXX	Traces	–	XX	XX	–	–	7.5YR 6/6 (reddish yellow)
SO 950	X	–	–	XX	X	–	XX	XX	–	–	5YR 6/6 (reddish yellow)
SO 1000	X	–	–	X	X	–	XX	XX	–	–	5YR 5/8 (yellowish red)
SO 1100	X	–	–	X	XX	–	XX	Traces	X	–	2.5YR 3/6 (dark red)
AQM	–	–	–	XXXX	–	–	X	X	–	Anl	–

for calcite),[28] might be due to the relatively short firing duration, causing a shift of decomposition reactions to higher temperatures.[42,43] As far as calcite is concerned, grain-size is another factor that could significantly affect its persistence at higher T (see micrographs in Section 3.2.2).

Starting from 800/850 °C, calcium oxide reacted with Al_2O_3 and SiO_2 available after phyllosilicates dehydroxylation to form melilite (gehlenite).[8,28,44–46] Reaction rims of melilite composition were observed at SEM-EDS already at 850 °C at the edges of decomposing carbonates (Fig. 3a). EDS analyses showed that these reaction rims were Mg- and Fe-rich gehlenites (Table 4). XRPD revealed that melilite reflection reached its maximum intensities between 950 and 1000 °C, a slightly

higher temperature than what was reported in other studies.[11,28] These results indicate that the only XRPD analysis must be carefully managed in the investigation of archaeological ceramics because phase breakdown (e.g., illite, calcite) and the formation of new minerals (e.g., gehlenite, clinopyroxene) are usually considered firing temperature markers.

At 1100 °C melilite decreased significantly, and other calcium silicates (e.g., Al-rich diopside),[47] which already formed starting from approximately 800 °C, developed further. In fact, the decomposition of carbonates also allowed the development of new Ca- (or Ca and Mg) silicate phases, wollastonite and diopside. SEM-EDS analyses (Table 5) showed that newly formed pyroxenes observed in this study revealed the composition of
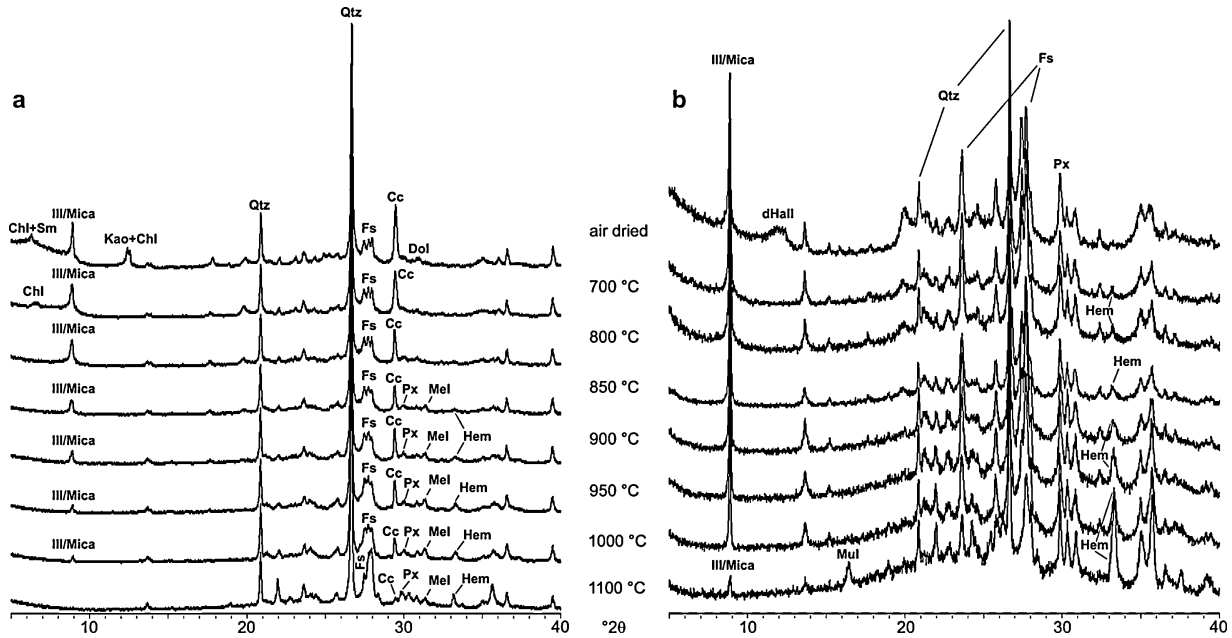
Fig. 2. XRPD patterns of raw and fired IS (a) and SO (b) samples. Abbreviations: Qtz, quartz; Fs, feldspar; Cc, calcite; Dol, dolomite; Px, pyroxene; Mel, melilite; Hem, hematite; Mul, mullite; Ill, illite; Sm, smectite; Kao, kaolinite; Chl, chlorite; dHall, dehydrated halloysite.

ferroan aluminian diopside.[46] The initial development of thin reaction rims tending to this composition was detected via SEM-EDS already starting from 800 °C (Fig. 3b). At this *T* the presence of pyroxene was also noticed in the XRPD pattern, then a slight rise of its reflection was recorded starting from 850 °C, whereas a tangible increase of pyroxene amount was observed at 1100 °C. This might also be due to the wollastonite formation by reaction between pre-existing gehlenite and quartz

(Fig. 3c).[45] These reaction rims assume a fingered geometry (Fig. 3c), a peculiar morphology occurring when two fluid or semi-plastic solids of different composition and viscosity are in contact.[28,48]

Among other Ca-silicates, we must point out the occurrence of newly formed cuspidine $[Ca_4Si_2O_7(F,OH)_2]$ observed at SEM-EDS between 900 and 1100 °C (Table 5). We detected cuspidine at the edges of silicates (feldspars and quartz) in
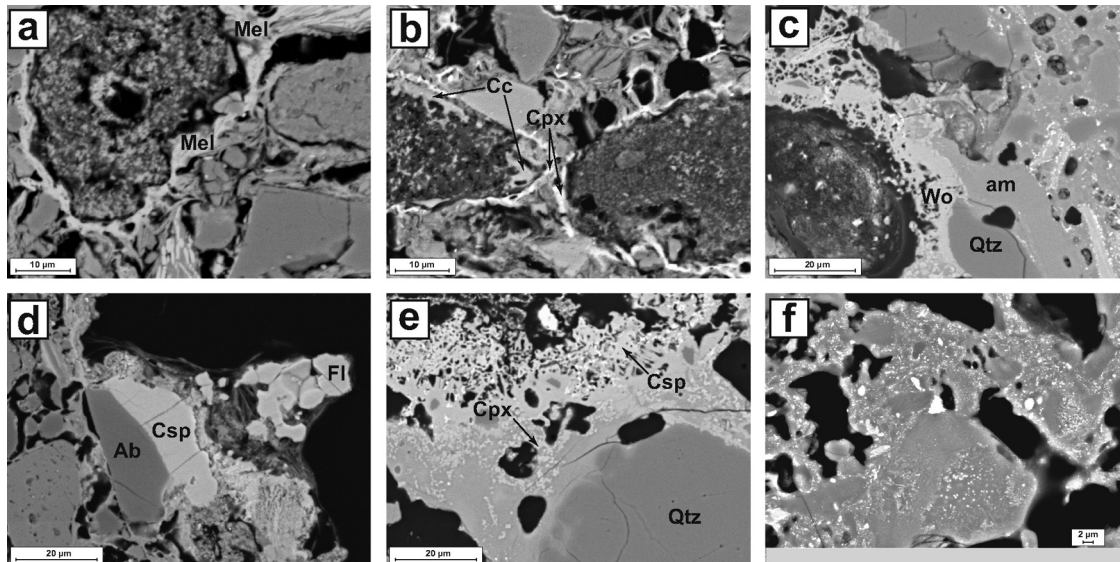

Fig. 3. Backscattered electrons SEM images of: (a) IS 850. Newly formed melilite (Mel) rim between carbonate and clay matrix. (b) IS-C 800. Thin reaction rims of clinopyroxene (Cpx; Al-rich diopside) composition. (c) IS 1100. Large reaction rim with fingered geometry of wollastonite (Wo) around a pre-existing carbonate in contact with quartz (Qz) and glassy amorphous phase (am). (d) IS-C 900. Newly formed cuspidine (Csp) on the edge of an albite (Ab) crystal in contact with carbonate mass and fluorite (Fl). (e) IS-C 1100. Newly formed cuspidine (Csp) and clinopyroxene (Cpx). (f) Backscattered electrons FESEM images of sample SO 1100. Iron oxides particles (white dots) in amorphous phase.

Table 4
Representative EDS-analyses (wt.%) and cation proportion (a.p.f.u.) of melilites in IS ceramics.

	Melilite IS 800	Melilite IS 800	Melilite IS 850	Melilite IS 900	Melilite IS-C 900	Melilite IS 950	Melilite IS 950	Melilite IS 950	Melilite IS-C 1000	Melilite IS-C 1100
SiO_2	33.69	32.93	31.74	31.58	39.54	32.85	37.44	33.16	36.01	34.09
TiO_2	0.48	1.39	0.55	0.01	0.44	0.15	0.22	0.75	0.40	0.26
Al_2O_3	16.42	17.90	16.78	21.91	16.33	15.93	14.55	20.96	15.72	19.44
FeO*	4.56	6.53	6.28	3.12	5.88	7.02	5.37	3.98	3.79	3.23
MnO	–	0.07	–	–	0.27	0.30	0.28	–	0.15	–
MgO	1.91	2.37	2.66	0.79	2.53	2.15	1.67	3.22	3.32	2.36
CaO	41.16	37.88	40.64	41.07	34.53	41.14	38.93	38.01	38.86	39.16
Na_2O	0.08	–	0.24	0.30	0.16	0.24	0.66	0.32	0.26	0.17
K_2O	0.42	0.35	0.37	0.61	0.12	0.05	0.21	0.20	0.08	0.10
F	–	–	–	–	–	–	–	–	–	–
Total	98.73	99.41	99.26	99.40	99.82	99.85	99.33	100.61	98.59	98.83

Numbers of ions on the basis of:

	14 (O)	14 (O)	14 (O)	14 (O)	14 (O)	14 (O)	14 (O)	14 (O)	14 (O)	14 (O)
Si	3.181	3.085	3.019	2.940	3.577	3.112	3.480	3.019	3.348	3.153
Ti	0.034	0.098	0.039	0.000	0.030	0.011	0.015	0.051	0.028	0.018
Al	1.828	1.976	1.880	2.404	1.741	1.779	1.593	2.249	1.723	2.119
Fe	0.360	0.512	0.500	0.243	0.445	0.556	0.418	0.303	0.295	0.250
Mn	–	0.005	–	–	0.021	0.024	0.022	–	0.011	–
Mg	0.269	0.330	0.378	0.110	0.341	0.304	0.232	0.437	0.460	0.326
Ca	4.164	3.802	4.141	4.096	3.347	4.176	3.877	3.707	3.870	3.881
Na	0.015	–	0.044	0.055	0.028	0.045	0.119	0.056	0.047	0.031
K	0.051	0.042	0.045	0.073	0.014	0.006	0.025	0.023	0.010	0.012
F	–	–	–	–	–	–	–	–	–	–
Total	9.903	9.850	10.046	9.921	9.543	10.013	9.780	9.845	9.792	9.791

Total Fe as Fe^{2+}

Table 5
Representative EDS-analyses (wt.%) and cation proportion (a.p.f.u.) of cuspidine, clinopyroxene, and wollastonite in IS ceramics.

	Cuspidine IS-C 900	Cuspidine IS-C 1000	Cuspidine IS-C 1000	Cuspidine IS 1100	Cuspidine IS-C 1100	Clinopyroxene IS 1000	Clinopyroxene IS 1100	Clinopyroxene IS-C 1100	Wollastonite IS 1100	Wollastonite IS-C 1100
SiO_2	31.63	31.82	32.11	30.97	32.63	43.42	42.76	44.33	51.31	52.84
TiO_2	–	–	–	–	–	0.23	0.98	0.73	–	–
Al_2O_3	–	–	–	–	–	19.95	15.05	17.77	–	–
FeO*	0.24	0.71	–	–	0.22	6.04	12.85	9.48	1.48	0.61
MnO	–	–	0.20	–	0.02	0.19	0.41	0.53	–	–
MgO	–	–	–	–	–	1.76	4.80	5.70	0.94	0.54
CaO	58.60	58.74	59.92	60.05	56.08	27.42	22.03	20.41	45.56	45.37
Na_2O	0.03	0.23	0.21	0.04	0.16	0.36	0.20	0.68	0.17	0.15
K_2O	0.10	0.01	0.06	–	–	0.20	0.72	0.28	0.25	–
F	8.92	8.69	8.02	8.33	10.91	–	–	–	–	–
Total	99.52	100.20	100.52	99.39	100.01	99.58	99.81	99.91	99.72	99.51

Numbers of ions on the basis of:

	8 (O, F)	8 (O, F)	8 (O, F)	8 (O, F)	8 (O, F)	6 (O)	6 (O)	6 (O)	18 (O)	18 (O)
Si	2.003	1.998	1.994	1.961	2.077	1.628	1.648	1.656	5.982	6.106
Ti	–	–	–	–	–	0.007	0.028	0.021	–	–
Al	–	–	–	–	–	0.882	0.684	0.783	–	–
Fe	0.013	0.037	–	–	0.012	0.189	0.414	0.296	0.144	0.059
Mn	–	–	0.011	–	0.001	0.006	0.013	0.017	–	–
Mg	–	–	–	–	–	0.098	0.276	0.317	0.164	0.093
Ca	3.975	3.952	3.986	4.075	3.824	1.102	0.910	0.817	5.690	5.617
Na	0.004	0.028	0.026	0.005	0.019	0.026	0.015	0.049	0.039	0.035
K	0.008	0.001	0.005	–	–	0.005	0.018	0.007	0.038	–
F	1.787	1.726	1.575	1.669	2.197	–	–	–	–	–
Total	7.790	7.742	7.596	7.710	8.130	3.938	3.989	3.956	12.057	11.911

Total Fe as Fe^{2+}

Table 6
Modal analysis of the temper (AQM) and of representative ceramics fired at 700, 900, and 1100 °C. Bold fonts indicate the contribution of AQM in tempered ceramics. Abbreviations: A-fs, alkali feldspar; Pl, plagioclase; Cpx, clinopyroxene; Pum, pumices; Sc, volcanic scoriae; VL, volcanic lithics; Ol, olivine; Cb, carbonates; ARF, Argillaceous Rock Fragments.

	A-fs	Pl	Cpx	Pum	Sc	VL	Ol	Mica	Cb	ARF	Other	Voids	Matrix	Volcanics
AQM	30.8	1.5	5.0	18.0	42.1	2.6	–	–	–	–	–	–	–	–
IS 700	5.8	–	0.1	5.2	0.2	0.0	–	1.7	1.0	0.5	–	3.6	82.0	–
IS 900	5.2	–	0.4	2.0	1.0	0.0	–	1.4	3.6	0.2	–	3.2	83.2	–
IS 1100	5.3	–	0.4	0.8	0.4	0.9	–	1.2	0.6	0.4	–	6.1	84.0	–
Average	5.4	–	0.3	2.7	0.5	0.3	–	1.4	1.7	0.3	–	4.3	83.0	–
IS-A 700	**3.8**	**0.0**	**0.3**	**3.1**	**3.0**	**1.0**	–	–	1.4	0.3	7.9	12.1	67.2	**11.3**
IS-A 900	**4.3**	**0.1**	**0.7**	**3.6**	**1.6**	**2.6**	–	–	0.3	1.0	10.1	5.2	70.4	**13.0**
IS-A 1100	**3.8**	**0.0**	**0.1**	**5.8**	**3.0**	**0.2**	–	–	0.3	0.0	9.2	6.9	70.7	**12.9**
Average	**4.0**	**0.0**	**0.4**	**4.2**	**2.6**	**1.3**	–	–	0.6	0.4	9.1	8.1	69.4	**12.4**
IS-B 700	**5.3**	**0.0**	**0.0**	**7.6**	**2.7**	**1.6**	–	–	1.3	0.5	7.4	10.2	63.4	**17.2**
IS-B 900	**5.8**	**0.1**	**0.3**	**6.2**	**6.4**	**2.1**	–	–	0.8	0.8	8.3	10.0	59.3	**20.9**
IS-B 1100	**4.7**	**0.0**	**0.2**	**9.2**	**5.0**	**0.6**	–	–	0.7	0.1	6.4	14.7	58.4	**19.7**
Average	**5.3**	**0.0**	**0.2**	**7.7**	**4.7**	**1.4**	–	–	0.9	0.5	7.4	11.6	60.4	**19.3**
IS-C 700	**6.3**	**0.3**	**0.8**	**8.2**	**6.7**	**1.8**	–	–	1.9	0.4	7.5	17.4	48.7	**24.0**
IS-C 900	**6.9**	**0.0**	**0.1**	**10.6**	**6.4**	**2.2**	–	–	1.1	2.1	8.0	7.4	55.2	**26.2**
IS-C 1100	**6.9**	**0.6**	**0.6**	**8.4**	**6.7**	**1.0**	–	–	0.8	0.4	7.7	19.3	47.5	**24.2**
Average	**6.7**	**0.3**	**0.5**	**9.0**	**6.6**	**1.7**	–	–	1.3	1.0	7.8	14.7	50.5	**24.8**
SO 700	2.6	0.2	2.5	3.9	3.0	0.1	0.0	–	0.3	1.7	–	8.2	77.5	12.3
SO 900	4.5	0.1	1.5	5.3	0.6	0.1	0.3	–	0.5	2.9	–	9.3	75.1	12.2
SO 1100	4.9	0.1	2.5	5.8	0.2	0.5	0.3	–	0.1	0.5	–	11.0	74.2	14.3
Average	4.0	0.1	2.1	5.0	1.3	0.2	0.2	–	0.3	1.7	–	9.5	75.6	12.9

contact with fluorite-bearing carbonate masses (Fig. 3d), likely formed according to the following reaction[49]:

$$3CaO + 2SiO_2 + CaF_2 \rightarrow \underset{\text{cuspidine}}{Ca_4Si_2O_7F_2}$$
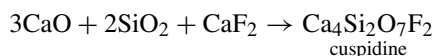
Newly formed cuspidine is reported in fluorite-bearing high-CaO ceramics generally from 850 to 1050 °C.[50] In this study cuspidine also occurred at the highest T (1100 °C) in association with other Ca-silicates (Fig. 3e).

At these maximum T (1100 °C) feldspar increase was detected by XRPD in the IS ceramics due to newly forming feldspars (e.g., anorthite) (Fig. 2a), in this case likely proceeding from the decomposition of gehlenite.[45] Although feldspar content increase was detected via XRPD at high T, it was not possible to analyse anorthite and/or other Ca-rich feldspars at SEM-EDS. Crystals were probably of very small size due to their incomplete development.

Newly formed hematite was detected via XRPD in both the IS and SO ceramics, which formed due to the oxidising firing atmosphere, and which also account for the reddish colour of the samples. In the IS samples this phase was present in traces from 700 up to 900 °C, while above these temperatures hematite reflections are more intense. Nevertheless, lower amounts of hematite were detected with respect to the SO samples (Fig. 2b) probably because the hematite crystallisation was hindered by the newly forming calcium silicates, which may incorporate iron in their frameworks.[45,51,52] For this reason the IS specimens showed a lighter reddish colour than the SO ceramics. In the latter samples, submicrometric particles dispersed in the glassy phase at 1100 °C, visible in BSE images (Fig. 3f) and not detectable by EDS, could be correlated to iron oxides.[51]

Mullite was detected in the SO ceramics at maximum firing T (1100 °C) after the decomposition of phyllosilicates.[28] Nevertheless, neither hematite nor mullite could be analysed at SEM-EDS because of their very small size. In addition to hematite and mullite, these ceramics did not show any other pyrometamorphic transformation.

3.2.2. Petrography and microstructure

Thin section observation and modal analyses (Table 6) broadly confirmed the mineralogy yielded by XRPD analyses. The non-tempered IS samples contained silt and very fine sand grains (10–100 µm), mostly represented by quartz, feldspars, white mica, and rare brown mica (Fig. 4a). Sporadic alkali-feldspar, rare clinopyroxene, and pumices occurred as well, occasionally of coarser size (Fig. 4b).

At the lowest firing T (700 °C) only minor textural changes were observed with respect to the unfired materials, and we only noticed phyllosilicates exfoliated along their basal planes due to dehydroxylation (Fig. 4c).[53] The ceramic matrix shows a weak optical activity up to 800 °C (Fig. 4a and b), successively obliterated by sintering at higher temperatures. From 700 to 900 °C the ceramic matrix showed a black core due to the short duration of firing at these temperatures, which hindered the complete oxidation of the whole ceramic body,[54] probably also favoured by the presence of organic matter.[43]

Carbonate fragments and sporadic microfossils (foraminifera, ostracoda)[55] occurred in the IS non-tempered ceramics with an average content of approximately 2% (Table 6), and their structure still remained intact at 700 °C
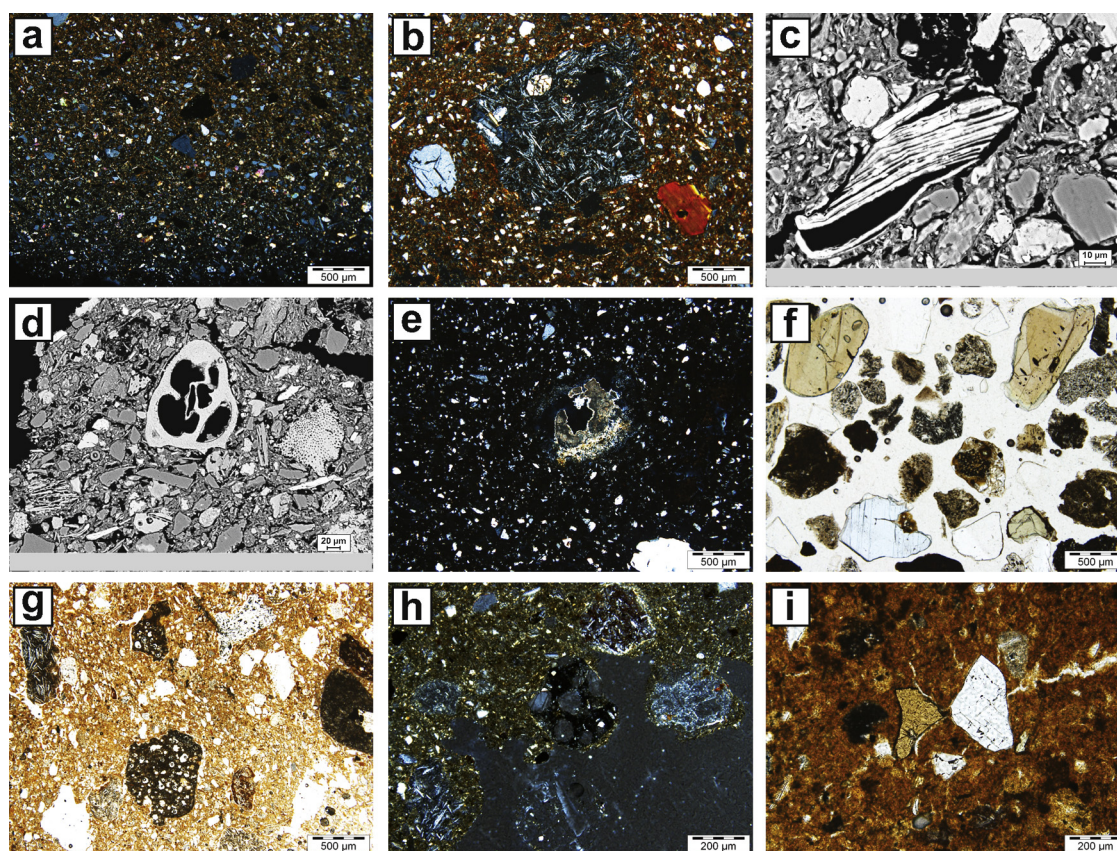
Fig. 4. PLM images of: (a) IS 700. Natural inclusions of IS ceramics (crossed polars). (b) IS 800. Sporadic large volcanic grain in non-tempered ceramics (crossed polars). Backscattered electrons FESEM images of (c) IS-C 700, exfoliated phyllosilicate for dehydroxylation, and (d)IS-C 700, carbonate microfossil. (e) IS 1100. Decomposed calcite (crossed polars). (f) AQM. Sand used as temper with alkali feldspar, clinopyroxene, pumices, and scoriae (parallel polars). (g) IS-C 700. Temper grains (pumices and scoriae) in the ceramic paste (parallel polars). (h) SO dry. Leucite-bearing scoriae (crossed polars). (i) SO 700. Garnet and alkali feldspar (parallel polars).

(Fig. 4d). As firing T increased, evidence of decarbonation occurred (Figs. 3a–c and 4e).

Tempered samples were characterised by the bimodal distribution of grains, in which the coarser fraction (generally over 250 μm) was mostly constituted by volcanic grains of the AQM sand (Fig. 4f). Uncoloured (diopside) and pale green clinopyroxene largely occurred in AQM temper, as is usually found in volcanic temper-bearing archaeological pottery from the Bay of Naples. Feldspars were represented by plagioclase and sanidine, the latter being the most abundant crystalline phase of the temper, as well as the most represented mineral of Phlegraean rocks.[38] Another feature of the tempered IS samples was the occurrence of abundant non-crystalline (glassy) volcanics such as pumices and scoriae (Fig. 4g).

Inclusions in SO samples were represented by pumice (∼5%), alkali feldspar (∼4%), clinopyroxene (∼2%), ARF (Argillaceous Rock Fragments; ∼2%), and volcanic scoriae (∼1%), often bearing leucite as well (Fig. 4h). Small lamellae of brown mica, sporadic crystals of altered olivine, magnetite, and garnet (Fig. 4i) were also observed, along with rare plagioclase. The observed paragenesis clearly suggests a Somma-Vesuvius origin.[56] Scattered rounded fragments of sandstones and rare carbonates also characterised these samples. The SO samples were composed on average by approximately 76% of the matrix,

showing optical activity up to 850 °C. The grains showed a bimodal distribution with an average content of approximately 15%. The fine fraction ranged from roughly 50 to 100 μm, while the coarse fraction ranged from 200 to 500 μm.

From the textural point of view, the IS specimens were strongly conditioned by temper content. Voids were mainly located around the temper grains and an increase of pores volume proportional to the temper amount was observed on the average of approximately 8% (IS-A), 12% (IS-B), and 15% (IS-C) (Table 6). The SEM images of freshly fractured samples, in fact, clearly showed discontinuities at the temper/matrix interface up to 1000 °C in the tempered samples (Fig. 5a).

Firing temperatures severely modified the ceramic microstructure. All the IS ceramics fired at 700 °C showed no significant structural modification and no vitrification. At 800 °C a better cohesion of particles, as an evidence of sintering, was observed, but still without vitrification (Fig. 5b). At 850 °C an initial vitrification started to occur, whereas at 900 °C an extended vitrification of the ceramic body developed and persisted up to 1000 °C. At the highest T (1100 °C) a continuous vitrification was observed: the glassy phase dramatically affected the whole ceramic body and pore morphology with the formation of large rounded and non-connected pores (Fig. 5c).
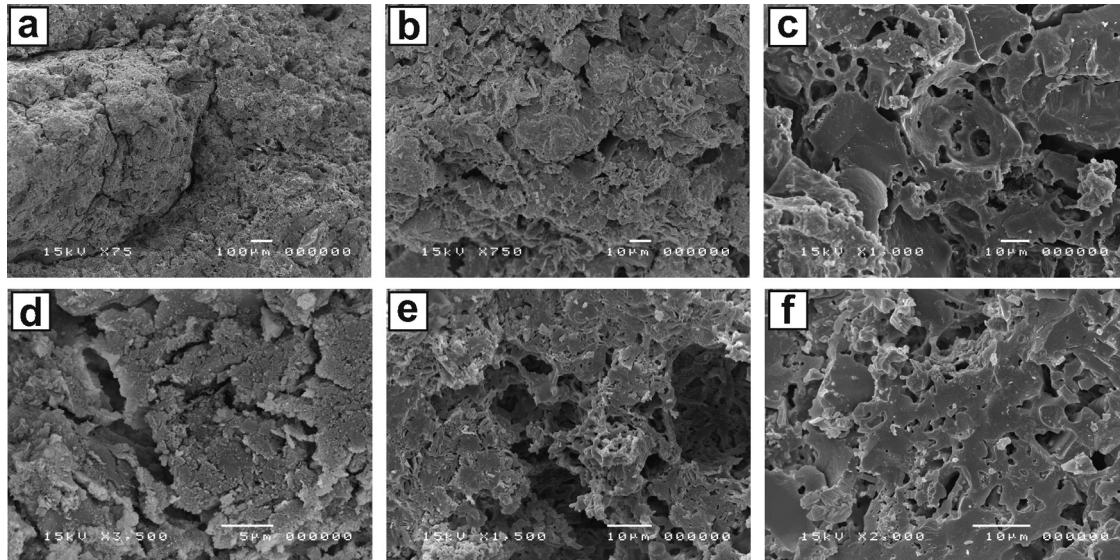
Fig. 5. SEM images of freshly fractured samples: (a) IS-C 1000. Discontinuities at temper/matrix interface. (b) IS 800. Poorly sintered structure. (c) IS-A 1100. Highly vitrified structure with rounded isolated pores. (d) SO 850. Poorly sintered structure. (e) SO 1000. Vitrified structure. (f) SO 1100. Continuous vitrification with non-connected pores.

The SO ceramics were characterised by a discontinued and poorly sintered microstructure up to 900/950 °C (Fig. 5d). Evolution of sintering and vitrification was rather progressive with the firing T. Starting from 1000 °C a well vitrified structure formed (Fig. 5e) and continuous vitrification characterised by large isolated pores, either rounded or elongated, developed at 1100 °C (Fig. 5f).

3.2.3. Physical characteristics
3.2.3.1. Study of the pore system.
Hydric tests showed that all IS samples fired at 1100 °C showed the lowest free water absorption (A_l, Table 7 and Fig. 6a), which is due to the low pore interconnection determined by the high degree of vitrification (revealed by SEM and PLM). A comparison between the free (A_l) and forced (A_f) water absorption values allowed us to examine how water circulates inside the pore system. This feature is graphically expressed by the slope of the curve comprised between A_l and A_f (Fig. 6a) which, in numerical terms, translates into higher A_x values when pores are scarcely interconnected[11] (Table 7). For this reason all ceramics fired at 1100 °C showed high A_x values, suggesting the existence of a closed porosity. MIP analyses (Table 7) showed that the IS samples were characterised by a unimodal pore size distribution and, from 700 to 1000 °C, by a displacement of the pore access radius towards larger sizes from approximately 0.5 to 1.0 μm (Fig. 6b). At 1100 °C pore size considerably increased (up to approximately 2.5 μm) due to the formation of large pores with the high degree of vitrification.

Furthermore, to a lesser extent, samples fired at the lowest temperatures (700, 800 °C) were characterised by relatively low A_l values (Table 7). MIP showed an increase of total porosity (P_t) in the range between 850 and 1000 °C (Table 7), probably as a consequence of the small contribution of microcracking which developed following the decomposition of carbonates ("lime blowing"),[57] likely not completely eliminated throughout the immersion in water immediately after firing.

Regarding the increasing amount of temper in the IS ceramics, within the T range (850–1000 °C) slight variations of A_l and A_f values were observed only in samples to which 20% and 30% of temper was added.

More interesting is a comparison of the hydric behaviour of the same samples at the same temperature, but at different amounts of temper. The tested samples achieved the lowest values of A_l, A_f, and O_p when the amount of added temper was equal to 10%. The same values significantly increased when the added temper was 20% and 30% (Table 7; Fig. 7a and b).

This behaviour could be due to different causes: the addition of 10% of temper improves the particle packing, reducing cracking and shrinkage of the unfired clay body. Higher temper percentages (20%, 30%) enhance discontinuities at temper/matrix interfaces.[11,58] This aspect could also explain the modification of the shape porosimetric curves as temper was increased, showing more symmetrical profiles, which spanned a wider size range (Fig. 6b). In fact, once the highest T is reached, the occurrence of continuous vitrification counterbalanced the effect of discontinuities at temper/matrix interfaces, thus determining a decrease of hydric parameters (Table 7).

For the drying test (Fig. 6a), the IS ceramics fired at minimum (700 °C) and maximum T (1100 °C) showed the fastest drying rate, especially in the first part of the test. The same samples showed the lowest values of drying index (D_i; Table 7). The drying rate is quite constant from 800 to 1000 °C for all IS samples, likely due to the presence of pores connected by microcracks.[10]

The SO ceramics were characterised by a gradual decrease of free (A_l) and forced (A_f) water absorption values, as well as absorption coefficient (C_a) and open porosity (O_p), as firing T increased (Fig. 6a and Table 7), which is due to the progressive evolution of both sintering and vitrification as observed by SEM and PLM. From 700 °C to 1000 °C these values were always higher than those observed for the IS ceramics fired at the

Table 7

P_t, total porosity (%); ρ_a, apparent density (g cm^{-3}); ρ_r, real density (g cm^{-3}) values of ceramics acquired via mercury intrusion porosimetry (MIP) along with hydric tests values of ceramics: A_l, free water adsorption (%); A_f, forced water adsorption (%); A_x, degree of pore interconnectivity (%); C_s, saturation coefficient (%); O_p, open porosity (%); ρ_a, apparent density (g cm^{-3}); ρ_r, real density (g cm^{-3}); C_a, absorption coefficient; D_i, drying index.

| Sample | Mercury intrusion porosimetry | | | | Hydric tests | | | | | | | | |
	P_t	ρ_a	ρ_r	A_l	A_f	A_x	C_s	O_p	ρ_a	ρ_r	C_a	D_i
IS 700	34.56	1.62	2.48	20.32	20.89	2.68	89.15	34.61	1.66	2.53	0.97	0.77
IS 800	28.02	1.50	2.08	20.15	21.15	4.70	85.10	34.30	1.62	2.47	0.97	0.79
IS 850	36.80	1.58	2.49	20.71	21.49	3.63	86.13	34.59	1.61	2.46	0.93	0.81
IS 900	36.87	1.57	2.49	21.51	22.87	5.94	82.08	36.31	1.59	2.49	1.07	0.82
IS 950	39.54	1.57	2.60	21.49	23.12	7.03	79.18	36.51	1.58	2.49	1.04	0.80
IS 1000	39.63	1.54	2.55	20.61	22.91	10.03	76.47	35.98	1.57	2.45	1.03	0.80
IS 1100	30.97	1.71	2.47	17.58	20.08	12.44	69.11	33.04	1.65	2.46	0.83	0.73
IS-A 700	31.09	1.69	2.45	18.54	19.23	3.55	86.54	32.91	1.71	2.55	0.78	0.77
IS-A 800	28.24	1.44	2.01	18.63	19.99	6.77	83.36	33.49	1.68	2.52	0.79	0.81
IS-A 850	34.26	1.57	2.39	17.80	18.60	4.30	83.32	30.88	1.66	2.40	0.70	0.80
IS-A 900	33.98	1.65	2.49	18.77	19.86	5.51	80.84	32.72	1.65	2.45	0.70	0.81
IS-A 950	35.77	1.62	2.52	19.22	20.66	6.97	78.85	33.88	1.64	2.48	0.83	0.79
IS-A 1000	37.94	1.61	2.52	19.37	20.95	7.53	77.62	34.05	1.63	2.47	0.91	0.80
IS-A 1100	31.89	1.70	2.50	17.04	19.27	11.59	68.83	31.89	1.65	2.43	0.75	0.75
IS-B 700	36.19	1.62	2.54	18.64	19.86	6.11	85.35	33.82	1.70	2.57	0.90	0.75
IS-B 800	35.14	1.70	2.62	18.68	20.08	6.96	83.19	33.68	1.68	2.53	0.93	0.78
IS-B 850	36.65	1.63	2.57	19.32	20.86	7.41	81.36	34.36	1.65	2.51	0.94	0.79
IS-B 900	37.66	1.66	2.66	19.67	21.32	7.71	80.80	35.06	1.64	2.53	0.91	0.80
IS-B 950	38.16	1.58	2.56	20.15	22.07	8.70	79.53	35.80	1.62	2.53	0.98	0.79
IS-B 1000	37.45	1.60	2.56	20.72	22.66	8.56	79.42	36.50	1.61	2.54	1.00	0.78
IS-B 1100	31.67	1.68	2.46	17.37	19.65	11.62	75.66	32.80	1.67	2.48	0.83	0.73
IS-C 700	28.68	1.68	2.35	19.17	20.85	8.04	84.34	35.14	1.69	2.60	0.93	0.76
IS-C 800	32.07	1.68	2.48	19.24	21.01	8.41	82.46	35.08	1.67	2.57	0.81	0.79
IS-C 850	29.72	1.70	2.42	19.56	21.39	8.57	82.56	35.36	1.65	2.56	0.90	0.80
IS-C 900	28.48	1.67	2.33	20.14	21.88	7.91	84.00	36.02	1.65	2.57	0.96	0.79
IS-C 950	31.98	1.66	2.44	20.81	22.70	8.32	82.63	36.83	1.62	2.57	1.00	0.78
IS-C 1000	33.82	1.62	2.45	20.91	22.81	8.33	82.91	36.99	1.62	2.57	0.97	0.79
IS-C 1100	28.47	1.72	2.41	17.88	20.43	12.55	79.87	34.09	1.67	2.53	0.79	0.73
SO 700	41.71	1.34	2.29	35.96	37.06	2.97	91.28	49.44	1.33	2.64	2.33	0.81
SO 800	45.01	1.38	2.51	34.98	35.63	1.83	92.08	48.75	1.37	2.67	2.04	0.83
SO 850	38.48	1.39	2.27	33.69	34.43	2.16	90.93	47.90	1.39	2.67	1.94	0.86
SO 900	44.22	1.40	2.51	33.20	34.28	3.15	89.31	47.81	1.39	2.67	1.91	0.85
SO 950	41.19	2.17	3.69	30.52	31.66	3.61	88.61	45.43	1.43	2.63	1.68	0.83
SO 1000	40.89	1.52	2.57	26.02	27.60	5.71	85.38	42.31	1.53	2.66	1.40	0.79
SO 1100	27.74	1.85	2.56	17.66	19.52	9.54	78.78	33.86	1.73	2.62	0.92	0.72

same temperatures, owing to the more porous structure of the SO ceramics. At maximum T (1100 °C) high vitrification reduced the water absorption to a value comparable to that of the IS ceramics fired at the same T. MIP curves were characterised by wide and irregular profiles, likely reflecting the high heterogeneity of this material. Samples fired up to 900 °C showed peaks in the fine pores range (0.01–0.1 μm) and tails spanning up to approximately 10 μm (Fig. 6b). Starting from 950 °C profiles became more symmetrical and pore-size distribution concentrates around large radii, progressively shifting from 1 μm at 950 °C up to approximately 10 μm at 1100 °C (Fig. 6b). At each firing T the drying behaviour was similar to that of the IS ceramics fired at the same T, and only the drying index (D_i) values were slightly higher than those of the IS ceramics fired in the range between 700 and 950 °C.

The saturation coefficient (C_s) generally tended to decrease with the firing temperature in all ceramic samples of this study, in this case due to the progressive vitrification, which hindered

the water penetration in the ceramic body. Note that the hydric values of SO and IS fired at 1100 °C were similar, suggesting that the high vitrification stage regulated the hydric behaviour of the two ceramics types.

3.2.3.2. Strength, toughness, and thermal behaviour. Firing dynamics and glass/phase formation also accounted for the elastic behaviour of the two investigated types of ceramics. The ultrasonic tests performed on the IS ceramics showed that all low T samples (700 °C) were characterised by the lowest ultrasound waves velocity (V_p and V_s; Table 8) and elastic moduli (E, G, and K; Table 8), owing to their poorly sintered structure. A significant increase of all these values (Table 8) was recorded up to 850 °C (Fig. 8a and b), suggesting the formation of a sintered structure as observed at SEM. The earlier sintering of the IS ceramics could be due to the different type and high abundance of clay minerals.[59] Moreover, the presence of CaO promotes the formation of a viscous flow at lower temperatures
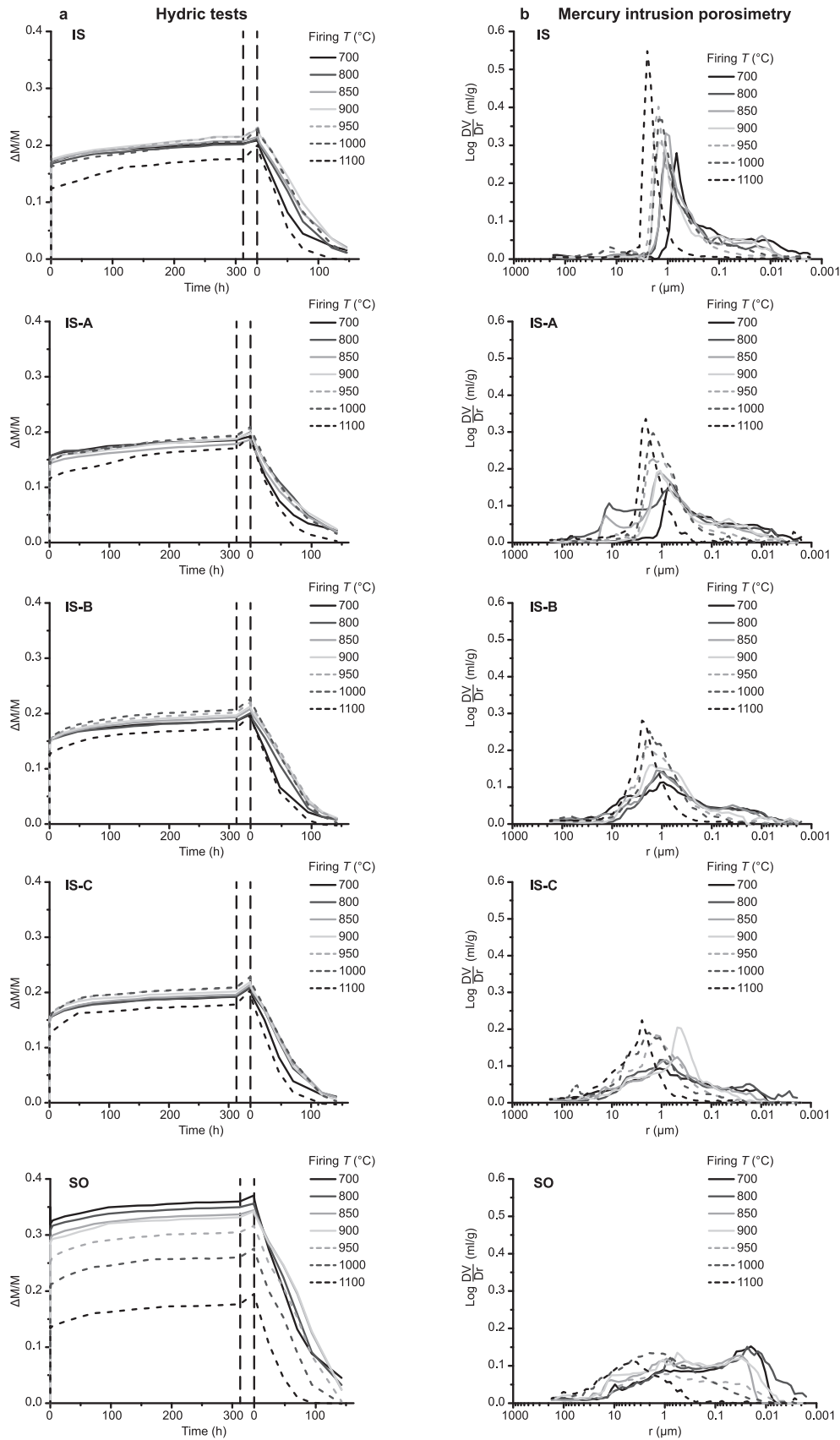
Fig. 6. (a) Mass change of fired samples due to free water absorption, desorption during hydric tests. (b) MIP pore size distribution curves of fired samples. Log differential intruded volume (ml/g) vs. pore radius (μm).
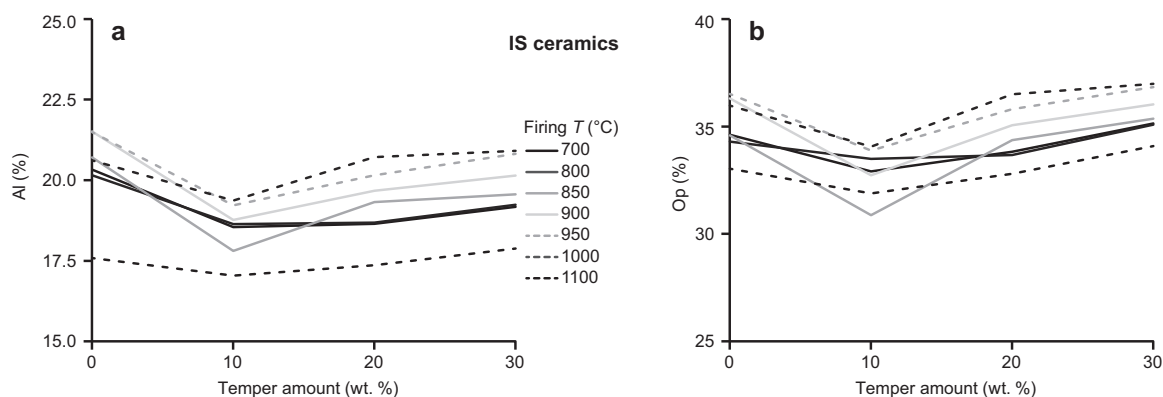
Fig. 7. Diagrams showing the variation of (a) free water absorption (A_l) and of (b) open porosity (O_p) for IS ceramics in relation with the temper percentage.

Table 8
Ultrasound wave velocity V_p (m/s) and V_s (m/s) of ceramics with elastic moduli: G, shear modulus (GPa); E, Young's modulus (GPa); K, bulk modulus (GPa).

	V_p	V_s	G	E	K
IS 700	1776	1113	2.06	4.64	2.16
IS 800	2213	1330	2.88	6.63	3.44
IS 850	2764	1610	4.19	9.93	5.47
IS 900	2830	1624	4.20	10.10	5.75
IS 950	2784	1634	4.22	9.97	5.39
IS 1000	2834	1600	4.04	9.81	5.77
IS 1100	3137	1804	5.38	12.88	7.29
IS-A 700	1812	1107	2.11	4.84	2.39
IS-A 800	2223	1316	2.92	6.88	3.64
IS-A 850	2760	1610	4.32	10.29	5.64
IS-A 900	2834	1656	4.52	10.75	5.84
IS -A 950	2861	1683	4.66	11.01	5.88
IS-A 1000	2739	1581	4.08	9.77	5.48
IS-A 1100	2855	1731	5.00	11.23	5.98
IS-B 700	1713	1053	1.90	4.34	2.11
IS-B 800	2256	1344	3.04	7.09	3.74
IS-B 850	2632	1502	3.73	8.98	5.20
IS-B 900	2700	1549	3.96	9.51	5.41
IS-B 950	2563	1472	3.53	8.44	4.84
IS-B 1000	2394	1370	3.04	7.23	4.20
IS-B 1100	2708	1576	4.18	9.92	5.53
IS-C 700	1558	905	1.39	3.30	1.87
IS-C 800	2068	1210	2.45	5.81	3.16
IS-C 850	2459	1404	3.27	7.85	4.57
IS-C 900	2393	1410	3.29	7.76	4.21
IS-C 950	2262	1295	2.75	6.61	3.78
IS-C 1000	2137	1246	2.53	6.04	3.32
IS-C 1100	2460	1336	2.99	7.40	4.81
SO 700	1240	719	0.69	1.65	0.91
SO 800	1320	776	0.83	1.96	1.05
SO 850	1417	840	0.98	2.31	1.23
SO 900	1444	899	1.13	2.57	1.19
SO 950	1735	1002	1.45	3.45	1.94
SO 1000	2046	1136	1.99	4.82	3.03
SO 1100	3017	1629	4.61	11.45	7.52

(700–850 °C)[60,61] and the initial formation of intercrystalline bonding among newly forming calcium silicates.[10] From 850 to 1000 °C ultrasound wave velocities and elastic moduli of non-tempered samples remained stable (Fig. 8a and b; Table 8). This

behaviour could be due to the formation of new mineral phases, which subtracting energy from the system inhibited further glass development.

The addition of 10% of temper did not affect the ultrasound velocity and elastic moduli; the same parameters show an overall decrease in samples with 20% and 30% of temper, likely due to the grain/matrix discontinuities, which caused dissipation of elastic energy, improving the toughness of the ceramics. In the same mixtures (20%, 30%) a further decrease of ultrasound velocity and elastic moduli were observed at increasing temperature from 900 to 1000 °C. As also seen in the pore system (see hydric parameters), this could be related to the sintering and shrinkage which, affecting the only ceramic matrix, leaves more space at temper/matrix interfaces.

The SO ceramics were generally characterised by elastic moduli lower than those of the IS ceramics, up to 1000 °C, likely due to their less cohesive and weaker structure, although a gradual increase of elastic moduli was noticed in the whole firing temperature range due to the progressive development of sintering. At the highest T the formation of glass was very intense and ultrasound velocity (V_p and V_s; Table 8) and elastic moduli (E, G, and K; Table 8) reached approximately the same values observed for the IS samples fired at the same T (Fig. 8a and b).

Infrared thermography showed that all ceramics fired at temperatures higher than 700 °C were characterised by a better heat propagation (Fig. 9a), due to the more dense and continuous ceramic structure.[62] Among the investigated samples, the IS ceramics showed a better thermal conductivity, which achieved its highest values at 900 °C. This is again a consequence of the well sintered structure of the IS ceramics at relatively low firing temperatures (850 °C), favoured by the intercrystalline bonds of newly formed calcium silicates as well.[62,63] The addition of temper did not provide appreciable differences in IRT observations.

Although the SO ceramics showed worse features such as lower strengths and higher water absorptions than the IS samples, the IRT test showed remarkable refractory properties of these ceramics, revealing their technological potential. Evident lower heat propagation of the SO ceramics was revealed by both lower height and heating/cooling displacement of the isotherm at IRT (Fig. 9b). The better refractory properties of the SO ceramics were due to their more discontinuous and porous ceramic
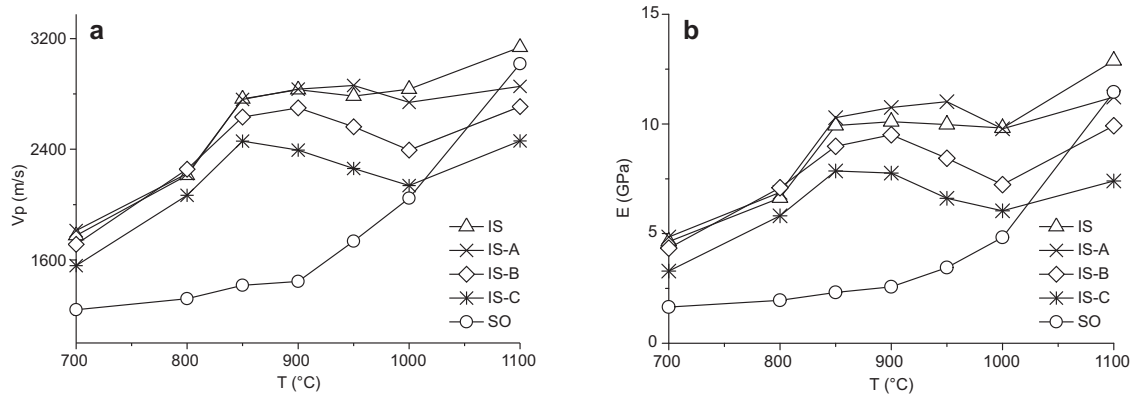
Fig. 8. Diagrams showing the variation of (a) ultrasound velocity (V_p) and (b) Young's modulus (E) vs. firing T.
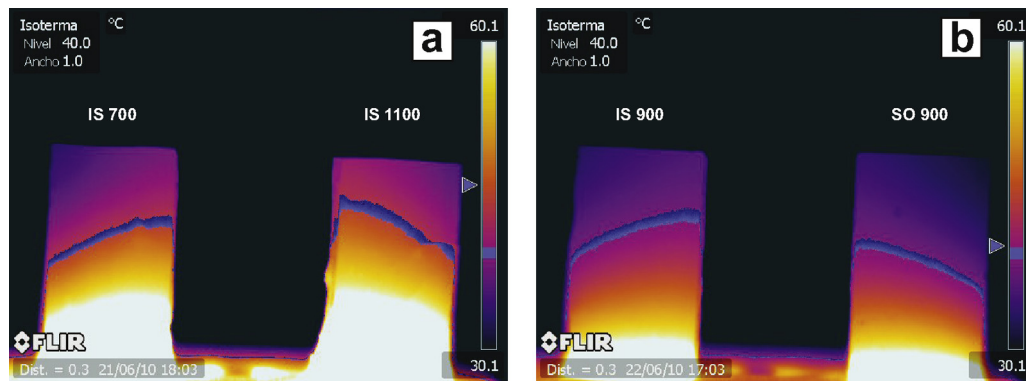

Fig. 9. Representative IR thermographic images representing the height of the isotherm after 20 min of heating in (a) high-CaO ceramics fired at 700 (IS 700) and 1100 C (IS 1100), and (b) high-CaO (IS 900) and low-CaO (SO 900) ceramics fired at the same T (900 °C).

body, likely favoured by the presence of pumices, which act as thermal insulators for their vacuolar structure.[64] Once a vitrified structure prevailed in the ceramic body of both the IS and SO samples fired at the highest T, similar heat propagation was recorded.

4. Conclusions

Experimental firing of the two clayey raw materials from the Bay of Naples area showed that the high-CaO ceramics from Ischia gain a more compact and hard structure starting from relatively low temperatures (∼850 °C). This feature makes this clay suitable for the production of ceramics at low temperatures with optimal strengths and with relatively short firing times (7–8 h), therefore requiring a low energy process.[65] In fact, a denser ceramic body with lower water absorption, possibly also through the use of coatings, favours the waterproof characteristics of the artefacts. In addition, high-CaO pastes yield a particularly stable microstructure over a wide temperature range (850–1000 °C), thus ensuring a consistent product quality, sparing the need for a strict control of firing conditions.[66]

The addition of temper resulted in different technological characteristics. With low percentages of temper (10%) most physical properties were almost unaffected. However a lower porosity and water absorption may support this technological choice for the realisation of hard/waterproof ceramics (e.g., tableware). This temper amount (10%) seems to represent the

best compromise to minimise the shrinkage attitude in the clay body and to improve the packing in the ceramic body. As the temper amount is increased to 20–30%, water absorption increases due to discontinuities at temper/matrix interfaces. These discontinuities, however, improve the dissipation of mechanical energy, providing better toughness to ceramic materials, which can better withstand shocks without breaking.[19] Therefore, the use of 20–30% of temper could be useful for pottery with a good balance between water resistance and toughness, such as transport amphorae, often stressed due to their specific use.

Ceramics made with the weathered pyroclastics from the Sorrento area are characterised by a less dense and less sintered ceramic body up to 1000 °C, compared to the ceramics from Ischia which were fired in the same temperature range. For this reason, this clayey material is not suitable to make ceramic products for which a certain resistance and hardness is required (e.g., tableware, amphorae). Moreover, the lower plasticity makes this clay difficult to work with and shape in elaborate forms.

On the contrary, ceramics from the Sorrento area showed some peculiar properties. Due to their porous and less dense structure, and to the natural presence of coarse-sized inclusions, these ceramics are characterised by low stiffness (as shown by low elastic moduli) and high toughness, resulting in a greater aptitude to absorb both thermal and mechanical energy.[19,67] Hence, they are very suitable for the production of heat resistant ceramics and refractory bricks. In particular, they show good thermal shock resistance when used for cooking with direct

flame contact, a characteristic which is also improved by the lower thermal expansion coefficient of low-CaO ceramics.[19] Moreover, their refractory properties allow a slow and uniform distribution of the heat to the food during cooking. For these reasons, this raw material is currently exploited to produce artisanal refractory bricks of superior quality, mainly used to build wood-burning ovens for cooking food, and bread and pizza in particular.

Low thermal conductivity is also enhanced by vacuolar inclusions such as pumices. Nevertheless, the presence of coarse pumices creates structural inhomogeneities, which would compromise the even distribution of the heat.[5] For this reason, SO raw materials are usually milled and mixed before moulding to obtain a more homogeneous structure and thermal conductivity.

Archaeological evidence shows that several (especially prehistoric) cooking wares produced with both high- and low-CaO clay types are characterised by toughness and thermal shock resistance when fired at relatively low temperatures (<850 °C),[68] but these products do not have the right strength and resistance to be durable. Our experiments proved that weathered pyroclastics show optimum thermal shock resistance and refractory properties even when fired at higher temperatures (850–1000 °C) necessary for stronger pottery.

Acknowledgements

References

1. De Bonis A, Grifa C, Cultrone G, De Vita P, Langella A, Morra V. Raw materials for archaeological pottery from the Campania Region of Italy: a petrophysical characterization. *Geoarchaeology* 2013;**28**(5):478–503.

2. Morel JP. La ceramica campana A nell'economia della Campania. In: *Napoli Antica, Catalogo della Mostra. Napoli (Italy).*; 1985. p. 372–8.

3. Morel JP. Remarques sur l'art et l'artisanat de Naples antique. In: *Neapolis. Atti del XXV CMGr, Taranto 3–7 ottobre 1985, Taranto (Italy).*; 1986. p. 305–56.

4. Grifa C, Morra V, Langella A, Munzi P. Byzantine ceramic productions from Cuma (Campi Flegrei, Napoli). *Archaeometry* 2009;**51**(1):75–94.

5. Morra V, De Bonis A, Grifa C, Langella A, Cavassa L, Piovesan R. Minero-petrographic study of cooking ware and Pompeian Red Ware (Rosso Pompeiano) from Cuma (Southern Italy). *Archaeometry* 2013;**55**(5):852–79.

6. Grifa C, De Bonis A, Langella A, Mercurio M, Soricelli G, Morra V. A Late Roman ceramic production from Pompeii. *J Archaeol Sci* 2013;**40**(2):810–26.

7. Giampaola D, Febbraro S, De Bonis A, Guarino V, Morra V, et al. The pottery workshop area at Piazza Nicola Amore, Naples. Black-glaze and common ware production: archaeology and archaeometry. In: Greco G, Cicala L, editors. *Archaeometry. Comparing Experiences, Quaderni del Centro Studi Magna Grecia*, 19. Naus Editoria: Università degli Studi di Napoli, Federico II. Pozzuoli (NA); 2014 [in press].

8. Peters T, Iberg R. Mineralogical changes during firing of calcium-rich brick clays. *Am Ceram Soc Bull* 1978;**57**:503–9.

9. Maniatis Y, Tite MS. Technological examination of Neolithic-Bronze Age pottery from central and southeast Europe and from the Near East. *J Archaeol Sci* 1981;**8**:59–76.

10. Cultrone G, Sebastián E, Elert K, de la Torre MJ, Cazalla O, Rodríguez-Navarro C. Influence of mineralogy and firing temperature on the porosity of bricks. *J Eur Ceram Soc* 2004;**24**:547–64.

11. Grifa C, Cultrone G, Langella A, Mercurio M, De Bonis A, Sebastián E, et al. Ceramic replicas of archaeological artefacts in Benevento area (Italy): petrophysical changes induced by different proportions of clays and temper. *Appl Clay Sci* 2009;**46**(3):231–40.

12. Brown RJ, Orsi G, de Vita S. New insights into late Pleistocene explosive volcanic activity and caldera formation on Ischia (southern Italy). *Bull Volcanol* 2008;**70**(5):583–603.

13. Buchner G, Rittmann A. *Origine e passato dell'isola d'Ischia.* Napoli (Italy): Macchiaroli; 1948. p. 77.

14. Buchner G. I giacimenti di argilla dell'isola d'Ischia e l'industria figulina locale in età recente. In: *Quaderno del Centro studi per la storia della ceramica meridionale. Bari (Italy).*; 1994. p. 17–45.

15. De Bonis A, Grifa C, Langella A, Mercurio M, Perrone ML, Morra V. Archaeometric study of Roman pottery from caudium area (Southern Italy). *Period Miner* 2010;**79**:73–89.

16. Guarino V, De Bonis A, Grifa C, Langella A, Morra V, Pedroni L. Archaeometric study on terra sigillata from Cales (Italy). *Period Miner* 2011;**80**:455–70.

17. Grifa C, Langella A, Morra V, Soricelli G. Pantellerian ware from Miseno (Campi Flegrei, Napoli). *Period Miner* 2005;**74**(1):69–86.

18. Capriglione C, De Bonis A, De Tommaso G, Guarino V, Iuliano M, Marino D, et al. Grandi dolii protostorici d'impasto dalla Calabria centromeridionale. Contributo allo studio cronotipologico, tecnologico e funzionale. *Rivista di Scienze Preistoriche* 2012;**62**:331–62.

19. Tite MS, Kilikoglou V, Vekinis G. Strength, toughness and thermal shock resistance of ancient ceramics, and their influence on technological choice. *Archaeometry* 2001;**43**(3):301–24.

20. ASTM Test designation D2217. *Standard practice for wet preparation of soil samples for particle-size analysis and determination of soil constants*, vol. 04.08. Philadelphia, USA: ASTM; 1985.

21. ASTM Test designation D422. *Standard test method for particle-size analysis of soils*, vol. 04.08. Philadelphia, USA: ASTM; 1972.

22. ASTM Test designation D421. *Standard practice for dry preparation of soil samples for particle-size analysis and determination of soil constants*, vol. 04.08. Philadelphia, USA: ASTM; 1985.

23. ASTM Test designation D4318. *Standard test methods for liquid limit, plastic limit, and plasticity index of soils*, vol. 04.08. Philadelphia, USA: ASTM; 1984.

24. ASTM Test designation D4943. *Standard test method for shrinkage factors of soils by the wax method*, vol. 04.08. Philadelphia, USA: ASTM; 1989.

25. BSI British Standard BS 1377-2. *Methods of test for soils for civil engineering purposes. Classification tests*. London, UK: British Standards Institution; 1990.

26. ASTM Test designation D2974. *Standard test methods for moisture, ash, and organic. Matter of peat and other organic soils*, vol. 04.08. Philadelphia, USA: ASTM; 2000.

27. ASTM Test designation C24 - 09. *Standard test method for pyrometric cone equivalent (PCE) of fireclay and high alumina refractory materials*, vol. 15.01. Philadelphia, USA: ASTM; 2013.

28. Cultrone G, Rodríguez-Navarro C, Sebastián E, Cazalla O, de la Torre MJ. Carbonate and silicate phase reactions during ceramic firing. *Eur J Miner* 2001;**13**:621–34.

29. Bish DL, Reynolds Jr RC. Modern powder diffraction. In: Bish DL, Post JE, editors. *Reviews in mineralogy*, vol. 20. Washington, DC: Mineralogical Society of America; 1989. p. 73–99.

30. Moore DM, Reynolds RC. *X-ray diffraction and the identification and analysis of clay minerals*. New York: Oxford University Press; 1997. p. 378.

31. Melluso L, Morra V, Brotzu P, Tommasini S, Renna MR, Duncan RA, et al. Geochronology and petrogenesis of the cretaceous Antampombato–Ambatovy complex and associated dyke swarm, Madagascar. *J Petrol* 2005;**46**:1963–96.

32. NORMAL 7/81. *Assorbimento dell'acqua per immersione totale. Capacità di imbibizione*. Rome, Italy: CNR-ICR; 1981.

33. RILEM TC 25-PEM. Recommended tests to measure the deterioration of stone and to assess the effectiveness of treatment methods. Commission 25-PEM: Protection et Erosion des Monuments. *Mater Struct* 1980;**13**(75):175–253.

34. NORMAL 29/88. *Misura dell'indice di asciugamento (Drying Index)*. Rome, Italy: CNR-ICR; 1988.

35. ASTM Test designation D2845. *Standard method for laboratory determination of pulse velocities and ultrasonic elastic constants of rock*, vol. 04.08. Philadelphia, USA: ASTM; 1983.

36. Cultrone G, Sebastián E, Cazalla O, Nechar M, Romero R, Bagur MG. Ultrasound and mechanical tests combined with ANOVA to evaluate brick quality. *Ceram Int* 2001;**27**:401–6.

37. Prassianakis IN, Prassianakis NI. Ultrasonic testing of non-metallic materials: concrete and marble. *Theor Appl Fract Mech* 2004;**42**:191–8.

38. Morra V, Calcaterra D, Cappelletti P, Colella A, Fedele L, de Gennaro R, et al. Urban geology: relationships between geological setting and architectural heritage of the Neapolitan area. In: Beltrando M, Peccerillo A, Mattei M, Conticelli S, Doglioni C, editors. *The Geology of Italy: tectonics and life along plate margins, J Virt Explorer, vol. 36, paper 27, Electronic Edition*. 2010., http://dx.doi.org/10.3809/jvirtex.2010.00261, available at: http://virtualexplorer.com.au/journal/2010/36

39. Adamo P, Violante P, Wilson MJ. Tabular and spheroidal halloysite in pyroclastic deposits in the area of the Roccamonfina volcano (Southern Italy). *Geoderma* 2001;**99**:295–316.

40. de' Gennaro M, Cappelletti P, Langella A, Perrotta A, Scarpati C. Genesis of zeolites in the Neapolitan Yellow Tuff: geological, volcanological and mineralogical evidence. *Contrib Miner Petrol* 2000;**139**:17–35.

41. Boynton RS. *Chemistry and technology of lime and limestone*. 2nd ed. New York, USA: John Wiley & Sons Inc; 1980. p. 578.

42. Dondi M, Ercolani G, Guarini G, Marsigli M, Venturi I. Evoluzione della microstruttura durante la cottura rapida di impasti per piastrelle porose. *Ceramurgia* 1995;**25**(6):301–14.

43. Maritan L, Nodari L, Mazzoli C, Milano A, Russo U. Influence of firing on ceramic products: experimental study on clay rich in organic matter. *Appl Clay Sci* 2006;**31**:1–15.

44. Dondi M, Ercolani G, Fabbri B, Marsigli M. Chemical composition of melilite formed during the firing of carbonate-rich and iron-containing ceramic bodies. *J Am Ceram Soc* 1999;**82**(2):465–8.

45. Rathossi C, Pontikes Y. Effect of firing temperature and atmosphere on ceramics made of NW Peloponnese clay sediments. Part I: reaction paths, crystalline phases, microstructure and colour. *J Eur Ceram Soc* 2010;**30**:1841–51.

46. Rathossi C, Pontikes Y. Effect of firing temperature and atmosphere on ceramics made of NW Peloponnese clay sediments: part II. Chemistry of pyrometamorphic minerals and comparison with ancient ceramics. *J Eur Ceram Soc* 2010;**30**:1853–66.

47. Dondi M, Ercolani G, Fabbri B, Marsigli M. An approach to the chemistry of pyroxenes formed during the firing of Ca-rich silicate ceramics. *Clay Miner* 1998;**33**:443–52.

48. Grapes R. *Pyrometamorphism*. New York, USA: Springer-Verlag LLC; 2006. p. 275.

49. Fukuyama H, Tabata H, Nagata K. Determination of Gibbs energy of formation of cuspidine ($3CaO\cdots2SiO_2\cdots CaF_2$) from the electromotive force method using CaF_2 as the solid electrolyte. *Metall Mater Trans B* 2003;**34**(3):307–11.

50. García-Ten J, Monfort E, Gomez P, Gomar S. Influence of calcite content on fluorine compound emissions during ceramic tile firing. *J Ceram Process Res* 2006;**7**:75–82.

51. Nodari L, Marcuz E, Maritan L, Mazzoli C, Russo U. Hematite nucleation and growth in the firing of carbonate-rich clay for pottery production. *J Eur Ceram Soc* 2007;**27**:4665–73.

52. Molera J, Pradell T, Vendrell-Saz M. The colours of Ca-rich ceramic paste: origin and characterization. *Appl Clay Sci* 1998;**13**: 187–202.

53. Rodríguez-Navarro C, Cultrone G, Sánchez-Navas A, Sebastian E. TEM study of mullite growth after muscovite breakdown. *Am Miner* 2003;**88**:713–24.

54. Cerdeño del Castillo J, Díaz Rubio R, Obis Sánchez J, Pérez Lorenzo A, Velasco Vélez J. *Manual de patologías de las piezas cerámicas para la construcción*. Toledo, Spain: Aitemin; 2000. p. 118.

55. Barra D, Cinque A, Italiano A, Scorziello R. Il Pleistocene superiore marino di Ischia: paleoecologia e rapporti con l'evoluzione tettonica recente. *Studi Geologici Camerti* 1992;**1**(special issue):231–43.

56. Joron JL, Métrich N, Rosi M, Santacroce R, Sbrana A. Chemistry and petrography. In: Santacroce R, editor. *Somma-Vesuvius C.N.R. Quaderni de La Ricerca Scientifica, 114, Rome Consiglio Nazionale delle Ricerche*. 1987. p. 105–74.

57. Laird RT, Worcester M. The inhibiting of lime blowing. *Br Ceram Trans J* 1956;**55**:545–63.

58. Kilikoglou V, Vekinis G, Maniatis Y, Day PM. Mechanical performance of quartz-tempered ceramics: part I, strength and toughness. *Archaeometry* 1998;**40**:261–79.

59. Kornilov AV. Reasons for the different effects of calcareous clays on strength properties of ceramics. *Glass Ceram* 2005;**62**(11–12): 391–3.

60. Cultrone G, Sebastián E, de la Torre MJ. Mineralogical and physical behaviour of solid bricks with additives. *Constr Build Mater* 2005;**19**: 39–48.

61. Chen GH. Sintering, crystallization, and properties of CaO doped cordierite-based glass-ceramics. *J Alloys Compd* 2008;**455**:298–302.

62. Lassinantti Gualtieri M, Gualtieri AF, Gagliardi S, Ruffini P, Ferrari R, Hanuskova M. Thermal conductivity of fired clays: effect of mineralogical and physical properties of the raw materials. *Appl Clay Sci* 2010;**49**(3):269–75.

63. Erker A. The thermal conductivity of the brick ceramic body (part 2). *Ziegelindustrie International* 2002;**55**(11):32–7.

64. Hossain KMA, Lachemi M. Thermal conductivity and acoustic performance of volcanic pumice based composites. *Mater Sci Forum* 2005;**480–481**:611–6.

65. Dondi M, Marsigli M, Venturi I. Microstructure and mechanical properties of clay bricks: comparison between fast firing and traditional firing. *Br Ceram Trans* 1999;**98**:12–8.

66. Papachristodoulou C, Gravani K, Oikonomou A, Ioannides K. On the provenance and manufacture of red-slipped fine ware from ancient Cassope (NW Greece): evidence by X-ray analytical methods. *J Archaeol Sci* 2010;**37**:2146–54.

67. Carter CB, Norton MG. *Ceramic materials: science and engineering*. New York, USA: Springer-Verlag LLC; 2007. p. 716.

68. Hein A, Müller NS, Day PM, Kilikoglou V. Thermal conductivity of archaeological ceramics: the effect of inclusions, porosity and firing temperature. *Thermochim Acta* 2008;**480**:35–42.